This is the post-print version of a paper published in Analytical Biochemistry

Three complementary techniques for the clarification of temperature effect on low-density lipoprotein-chondroitin-6-sulfate interaction

Geraldine Cilpa-Karhu[a]*, Katriina Lipponen[a], Jörgen Samuelsson[b], Katariina Öörni[c], Torgny Fornstedt[b], Marja-Liisa Riekkola[a]*

[a]Laboratory of Analytical Chemistry, Department of Chemistry, P.O. Box 55, FIN-00014 University of Helsinki, Helsinki, Finland, [b]Department of Engineering and Chemical Sciences, Karlstad University, SE-651 88 Karlstad, Sweden and [c]Wihuri Research Institute, Haartmaninkatu 8, FIN-00290 Helsinki, Finland

*Correspondence: Prof. Marja-Liisa Riekkola and Dr. Geraldine Cilpa-Karhu, Laboratory of Analytical Chemistry, Department of Chemistry, P.O. Box 55, FIN-00014 University of Helsinki, Finland. E-mail: marja-liisa.riekkola@helsinki.fi and geraldine.cilpa@helsinki.fi. Fax: +358 9 19150253

Running title: Temperature effect on LDL-C6S interaction

ABSTRACT

A rigorous processing of adsorption data from quartz crystal microbalance technology was successfully combined with the data obtained by partial filling affinity capillary electrophoresis and molecular dynamics for the clarification of the temperature effect on the interaction of a major glycosaminoglycan chain chondroitin-6-sulfate (C6S) of proteoglycans with low-density lipoprotein (LDL), and with a peptide fragment of apolipoprotein B-100 (residue 3359-3377 of LDL, PPBS). Two experimental techniques and computational atomistic methods demonstrated a non-linear pattern of the affinity of C6S at temperatures above 38.0 ℃ to both LDL and PPBS. The temperature affects the interaction of C6S with LDL and PPBS either by influencing the structural behavior of glycosaminoglycan C6S and/or that of LDL.

Introduction

Atherosclerosis is an inflammatory disease initiated by the retention and accumulation of apolipoproteinB-100 (apoB-100) containing lipoprotein–derived lipids into the arterial wall. In particular, two interacting components have been recognized as determining counterparts in the pathogenesis, low-density lipoprotein (LDL) and chondroitin-6-sulfate rich arterial proteoglycan (C6S-PG) [1-3]. C6S belongs to the family of glycosaminoglycans and inherits a highly charged polysaccharide structure composed of alternating β-D-glucuronic acid (GlcUA) and 2-acetamido-2-deoxy-β-D-acetylgalactose (GalNAc-6-sulfate) monosaccharides. Besides participating in atherosclerosis, C6S and its derivates have been proven to have pathophysiological implications in a large variety of diseases e.g. in osteoarthritis, lung cancer, breast tumor [4-6]. In addition, even subtle differences amongst glycosaminoglycan structures could lead to specific pathophysiological behaviors. Therefore, studies on glycosaminoglycans and their interactional behavior are of high importance for a better understanding of their functions.

The strong affinity between LDL and C6S, which leads to insoluble complex formation, has been proven to arise from C6S affinity to positively charged regions of apoB, underlying the importance of specific segments of the protein part of LDL particle. Consequently, the surface charge of LDL is an important modulator of the interaction with the arterial proteoglycans. Uptake of LDL by arterial cells, particularly by macrophages, can lead to formation of foam cells and to the production of pro-inflammatory markers [7-12]. The increased inflammatory burden of the arterial wall may yield local extracellular acidification and increase in local temperature [13-14]. The acidic pH associated with thick, lipid-rich atherosclerotic lesions enhances the interaction of LDL with arterial wall proteoglycans [15-17]. This shows that the

3

inflammatory process itself and the derived responses contribute to the progression of atherosclerosis. Could the increased temperature also be pro-atherogenic? What is the effect of the increased temperature on the interaction of LDL with arterial proteoglycans, in particular in the 37.0-40.0 ˚C range? Most experimental data on LDL-PG interactions have been reported at 37.0 ºC. In addition, no atomistic theoretical study on the possible effect of temperature on LDL-C6S interaction has been reported earlier. To help in the clarification of the temperature effect on apoB-100-containing lipoproteins interaction with C6S, three methods, quartz crystal microbalance (QCM) utilizing adsorption energy distribution (AED) calculations, partial filling affinity capillary electrophoresis (PF-ACE) and atomistic molecular dynamics (MD) simulations were employed. These approaches have been successfully applied in our previous study for the clarification of interactions between apoB-100 peptide fragments and C6S [18]. With the new tool, AED-calculations, the degree of heterogeneity of the adsorption can be determined prior to the rival model fitting procedure. The LDL particle and a well-selected peptide fragment corresponding to the residues 3359-3377 of apoB-100, were used in this study. This peptide fragment has been identified as the main proteoglycan binding site (PPBS) [19].

The three methods demonstrated that temperature affects LDL-PG interaction and a temperature dependence pattern was put in evidence for temperatures above 37.0 ° C.

Materials and Methods

Chemicals and materials. 1-ethyl-3-(3-dimethylaminopropyl) carbodiimide hydrochloride (EDC, E 1769), N-(2-Hydroxyethyl)piperazine-N'-(2-ethanesulfonic acid) (HEPES), sodium meta-periodate, chondroitin-6-sulfate (M: 56 kDa), 11-mercaptoundecanoic acid (11-MUA) and PBS-tablets were purchased from Sigma (Darmstadt, Germany), sodium hydroxide (1.0

M), hydrochloric acid (1.0 M) were from FF-Chemicals (Yli Ii, Finland), and NaCl from J.T.Baker (Mallinckrodt, Baker, Deventer, the Netherlands). Sodium cyanoborohydride and carbohydrazide was obtained from Fluka (Buchs, Switzerland), acetic acid was from Merck (Darmstadt, Germany). Dimethyl sulfoxide (DMSO) was purchased from OY FF-Chemical Ab (Yli-Ii, Finland). The peptide fragment of apoB-100, PPBS, was synthesized at the Meilahti Protein Chemistry Facility and analyzed at the Protein Chemistry Core Facility, both at Biomedicum, University of Helsinki, Finland. The peptide was purified in a C18 reversed-phase column (Supelco Discovery wide-pore) with 10 column volumes of 0–70% (v/v) acetonitrile/H_2O gradient and quality controlled by MALDI-TOF/TOF mass spectrometry (AutoFlex III, Bruker) [20].

Quartz crystal microbalance (QCM) experiments.

Equipment. Attana A-100 QCM biosensor with Low Nonspecific Binding (LNB)-carboxyl coated and gold plated chips (Attana AB, Stockholm, Sweden) was used in QCM experiments [18,21]. The integrated Attester program was used to record the frequency shifts which represent the binding response of the analyte to the biosensor. MeterLab PHM 220 pH meter (Radiometer, Copenhagen, Denmark) was used in the pH measurements. Distilled water was further purified with a Millipore water purification system (Millipore S.A., Molsheim, France).

Sample and buffer preparation. Phosphate buffer saline tablets were used for the preparation of the PBS buffer (pH 7.4, ionic strength of 10 mM containing 2.7 mM KCl and 137 mM NaCl). PBS buffer and phosphate buffer (pH 7.4, ionic strength of 10 mM containing 25 mM NaCl) were used in the interaction studies. Acetate buffers (pH 4 and 5.5, ionic strength of 10 mM), and HEPES buffer (pH 7.4, ionic strength of 10 mM containing 150 mM NaCl) were prepared for the amino- and aldehyde-coupling procedures. The solutions of 0.2 M EDC, 0.05

5

M sulfo-NHS and 5 mM carbohydrazide were prepared in HEPES buffer and the solution of 0.1 M cyanoborohydride was prepared in acetate buffer (pH 4).

Coupling of C6S on LNB-carboxyl surface. C6S was coupled to LNB-carboxyl chip via aldehyde coupling. The sensor chip was first prewetted ex-situ with 20 µL of Milli-Q water and then, left to stabilize in the instrument in HEPES buffer, at a flow rate of 25 µL/min. For the immobilization of C6S, a flow rate of 10 µL/min was used. The surface of the chip was activated by three successive injections of a freshly-made mixture of (1:1, v:v) of EDC and sulfo-NHS solutions for 300 seconds (s) each, followed by three injections of a solution of 5 mM carbohydrazide for 200 s each. C6S was then oxidized by adding 2 mg of sodium meta-peroxide to 1 mL of C6S solution of 8 mg/mL prepared in acetate buffer (pH 5.5). Oxidized C6S (ox-C6S) was then coupled to the surface of the chip by making six injections of ox-C6S solution, for 350 s. Non-bounded ox-C6S were deactivated by injecting sodium cyanoborohydride (0.1 M) for 200 s. The C6S coupled on LNB was then ready for PPBS-C6S studies. PBS buffer   was used to stabilize the chip.

Coupling of C6S on gold surface. The previous procedure (C6S coupled on LNB chip) was not adapted to the study of the full LDL particle due to difficulties in regenerating the chip between runs. Therefore, the consideration of a linker between the chip and C6S appeared to be a better alternative. 11-mercaptoundecanoic acid (11-MUA) has been successfully employed to the immobilization of DNA on gold surfaces [22] and was chosen as a linker for our studies. 11-MUA was attached on gold surface according to the manufacturer instructions. Briefly, a beaker was washed three times with $H_2O:NH_2:H_2O_2$ (5:1:1, v:v:v) for 20 min at 70 °C. The third time, a gold-plated quartz crystal chip was inserted and the solution was left to boil for 10 min. The chip was then rinsed with milli-Q water and EtOH, and was left to incubate at 4 °C for 24 h in a vial containing 10 mM of 11-MUA solution. A last rinsing was necessary before insertion of the chip into the instrument.

6

C6S was amino-coupled to 11-MUA coated surface with the procedure reported previously [18]. Shortly, the inserted 11-MUA-modified chip was left to stabilize in 10 mM HEPES buffer at a flow rate of 25 µL/min. The latter was then decreased to 10 µL/min for the immobilization step. A freshly-made mixture of (1:1, v:v) of EDC and sulfo-NHS solutions was injected three times for 300 s each, then the C6S solution prepared in acetate buffer (PH 4) was injected three times for 300 s and at last, ethylene diamine solution was injected once for 300 s. C6S immobilized on 11-MUA gold-plated chip was then ready for LDL–C6S studies. The phosphate buffer was used to stabilize the chip.

LDL-C6S and peptide-C6S interaction studies at different temperatures. All experiments were carried out by injecting 35µL of the LDL/peptide solution at a flow rate of 25µL/mL.

The LDL-C6S interaction experiments were carried out at temperatures 37.0, 38.0, 39.0 and 40.0 ℃. Human LDL (d = 1.019–1.050 g/mL) was isolated from the plasma of healthy volunteers (Finnish Red Cross) by sequential ultracentrifugation in the presence of 3 mM EDTA [23-24]. Lowry method [25], with bovine serum albumin as standard, was used to determine the LDL concentration. LDL concentration [LDL] of 5 µg protein/mL was used at all temperatures, except at 37.0 ℃ where [LDL] was 1 µg protein/mL.

For PPBS-C6S interaction study, the experiments were performed at 25.0, 28.0, 34.0, 37.0, 38.0, 39.0 and 40.0 ℃. The peptide concentration ranged from 5.3 µM to 320 µM. To increase the accuracy of the data all PPBS-C6S experiments were made three times.

In this study, we assume that the Sauerbrey relation is valid and that the QCM frequency shifts are proportional to the adsorbed amount of solute [26].

Estimation of kinetic rate constants and affinity. The interaction strength between C6S and human LDL was pre-estimated with kinetic analysis using ClampXP software [27]. To gain more control of the data, the evaluation of kinetic rate constants was also performed using in-

house written program that describes a simple ligand-analyte adsorption desorption process implemented using python 3.3.0, numpy 1.7.0, scipy 0.11.0 and matplotlib 1.2.0.

Adsorption isotherm and adsorption energy distribution calculations. The LDL data were processed using the common kinetic analysis. We choose to use steady state approche for the peptides-C6S adsorption because using kinetic analysis one has to assume adsorption model prior the determination of equilibrium constants.

An adsorption isotherm describes the relationship between adsorbed and free concentration of the solute at constant and specific temperature [28-30]. The most simple adsorption model is the Langmuir model:

$$\Delta f = \frac{\Delta f_{max} K_a C}{1 + K_a C}$$

(1)

where Δf, Δf_{max}, C, and K_a are the measured QCM frequency shift, maximum frequency shift for saturated surfaces, injected solute concentration and the association equilibrium constant, respectively [31]. The Langmuir model describes homogenous interactions from an energetic point of view; however adsorption is most often heterogenic. The simplest model describing heterogenic interactions is the bi-Langmuir model consisting of two kinds of adsorption sites, the model is just a sum of two Langmuir terms. The degree of heterogeneity in the energy of interactions can be estimated prior to the model selection procedure, by calculating the adsorption energy distribution (AED) [29,31]. This is done by expanding the Langmuir adsorption isotherm model into a continuous distribution of independent homogeneous sites across a certain range of adsorption energies,

8

$$\Delta f(C) \;=\; \int_{K_{min}}^{K_{max}} f(\ln K_a)\,\theta(C,\,K_a)\,d\ln K_a$$

$$\theta(C,\,K_a) \;=\; \frac{K_a C}{1 + K_a C}$$

(2)

where $\theta(C, K_a)$ is the local adsorption model and $f(\ln K_a)$ is the AED. K_{min} and K_{max} are set to $1/C_{max}$ and $1/C_{min}$, respectively, where C_{min} and C_{max} are the lowest and highest sample concentration used in the QCM experiments. The AED was calculated using the expectation maximization method where the integral equation is discretized to a sum and iteratively solved [32].

Processing QCM data. First, adsorption isotherms were acquired under a very broad concentration range of the solute; this is because at different concentration levels different adsorption sites dominate. The determined adsorption datasets for each temperature were analyzed using a three-step procedure prior the model selection [29-31]. To start, (i) Scatchard plots were done (plotting $\Delta f/C$ vs Δf) to get a preliminary insight about the adsorption characteristics. Second, (ii) AEDs were calculated to determine the degree of heterogeneity, number of different adsorption sites. After steps (i) and (ii), only a few trustworthy models remain for the final step. Finally, (iii) fitting of rival models to the raw data and to their statistical evaluation using F-test (95%). This procedure gives a much more reliable estimation of the interactions as compared to the traditional approach consisting of a direct fitting to an adsorption isotherm model.

To exemplify steps (i) and (ii), Scatchard plots and AED are shown in Fig. 1 for three different adsorption isotherm data sets. If we inspect only the Scatchard plots (Fig. 1a), we can see that the Scatchard plot is linear for Dataset 1 and concave for Dataset 2 and 3. Linear Scatchard plots are only true for the Langmuir model. Concave Scatchard plots could be described with many different models such as Tóth and the bi-Langmuir models. The Tóth

model describes an adsorption where only one type of interaction exists but where there is heterogeneity revolved around this interaction [33] compared to bi-Langmuir where the adsorption heterogeneity is due to that two distinct adsorption sites with different adsorption energy are present. However, we cannot based simply on traditional tools for model fitting distinguish between bi-Langmuir and Tóth adsorption model. If we complement the analysis by AED calculations (Fig. 1b), we can see that Dataset 1 and Dataset 2 result in unimodal AED and Dataset 3 results in bimodal AED. With the combined information, we could stipulate that: Dataset 1 is most probably described with the Langmuir model, Dataset 2 is described with an adsorption model with unimodal heterogeneous AED, e.g. Tóth, and Dataset 3 is described with an adsorption model which has bimodal AED, e.g. the bi-Langmuir model. With this information it is much simpler to select a proper adsorption model candidates prior the model fitting.

Partial-filling affinity capillary electrophoresis (PF-ACE) experiments.

Equipment. Hewlett-Packard 3^D CE system (Agilent, Waldbronn, Germany) equipped with a diode array detector, an air-cooling device for capillary and a water bath for samples was used for the PF-ACE experiments. Bare fused-silica capillaries (i. d. 50 µm, o.d. 375 µm) were purchased from Optitronis GmbH, Kehl, Germany. The capillaries were cut to a total length of 38.5 cm and the detector window was burned to 30.0 cm.

Sample and buffer preparation. The sodium phosphate buffer with ionic strength of 20 mM was made by mixing phosphoric acid and sodium hydroxide until the pH reached 7.4.

Pre-coating procedure. Compared to our previous study [18] carried out by partial filling method a new, more robust pre-coating [34] was used in the present study. The negatively charged capillary wall was first coated at 25 ℃ with quaternized diblock-copolymer poly(*N*-2-methylvinylpyridinium iodide-*block*-ethylene oxide) (P2QVP-*b*-PEO) to minimize the EOF and adsorption of lipoproteins on the capillary wall. The coating procedure was fast and took

10

only 3.5 hours including the pretreatment. First, the capillary was successively pretreated using 1 M HCl for 20 min, 0.1 M HCl for 10 min, Milli-Q water for 25 min, and the solution of phosphate buffer for 5 min. Then, the capillary was flushed with P2QVP-b-PEO solution (0.1 mg/mL in phosphate buffer, pH 7.4, ionic strength 20 mM) for 60 min using 1 bar pressure, filled with the P2QVP-b-PEO solution and left to react for 30 min. After the coating step, the capillary was flushed 60 min with the phosphate buffer. The EOF was tested using Williams and Vigh method [35] and using DMSO as EOF marker. The EOF measured at 25 ℃ ranged from 1.9 x10^{-10} to 5.6 x 10^{-10} m^2/(V s), showing a quasi-neutral capillary inner-surface.

Partial filling procedure. The partial filling method followed the procedure described in our earlier studies [18,36]. First, the analytes were introduced hydrodynamically. Slightly negatively charged LDL (0.1 mg/mL) was introduced to the neutral capillary for 2 s under 50 mbar pressure, then 30 s plug of phosphate buffer was added. Next, C6S (0.6 mg/mL) was injected for the different time periods (1, 2, 3, 4, 5 and 6 s). Finally, a voltage of -25 kV was applied and both LDL and C6S started to move towards the anode located at the detector end. The detection was done at 200 nm. After each run the capillary was equilibrated with 2 min flush of phosphate buffer.

The affinity constants were calculated according to our previous studies [18] using Eq. 3

$$K_a = \frac{t_{total}}{t_{LDL} \cdot C_{C6S} \cdot V_{C6S}} \cdot \frac{d\Delta t}{d\Delta t_{filling}} \quad , \tag{3}$$

Where t_{total} is the time of C6S to reach the detector under 50 mbar pressure, Δt is the change in migration time of the complex, t_{LDL} is the migration time of LDL when C6S is not present, $\Delta t_{filling}$ is the filling time of C6S, C_{C6S} is the concentration of C6S, and V_{C6S} is the apparent volume of C6S calculated with the help of asymmetric field flow fractionation [37]. V_{C6S} was

11

set to 0.5 mL/mol. The PF-ACE experiments were carried out, just like those of QCM at 37.0, 38.0, 39.0 and 40.0 ℃.

Molecular dynamics (MD) calculations. A dodecasaccharide chain of chondroitin-6-sulfate (C6S) glycosaminoglycan [38], containing six repeats of GlcUA β(1→3) GalNAc-6-sulfate disaccharides joined by β(1→4) glycosidic linkages was used for the MD simulations. The apoB-100 peptide fragment of interest is the corresponding 19 amino acid peptide derived from the PPBS, residues 3359-3377, RLTRKRGLKLATALSLSNK.

Discovery studio 2.0 [39] was used to model C6S, PPBS and to obtain a starting conformation of C6S-PPBS system. A starting distance $d_{0,pulling}$ of 0.4 nm was set between C6S and PPBS center of masses. Two important points to be mentioned here are 1) PPBS starting structure is chosen to be helical in accordance to recently published data on the structure-dependence of PPBS on its interaction efficiency with C6S [40]. At the starting distance $d_{0,pulling}$, the helicity of PPBS still holds and is a good approximation and 2) The charge states of both C6S and PPBS were chosen to represent the physiological pH. Accordingly, C6S and PPBS were highly charged and held a net charge of -12 and +6, resp. The GROMACS 4.0.7, atomistic molecular dynamic simulation package, was used [41]. For all the simulations, explicit solvent model, in particular the SPC water model [42] was used. A minimum salt concentration of 200 mM, as required for the stability of small peptides [43] was considered. Details of the united-atom force field designed for C6S has been published elsewhere [38].

Potential of mean force (PMF). For the PMF calculations, pull code with constraint distances between C6S and PPBS center of masses was performed. The slow growth method was first carried out to obtain the C6S-PPBS system at fixed pulling distances. The system was pulled with a small velocity until 4.5 nm, generating up to 80 distance constraints. Seven temperature-dependent PMF calculations were carried out at 28.0, 34.0, 38.0, 38.5, 39, 39.5

and 40.0 ºC. For each temperature, all constraints were run separately with a minimum of 5 ns MD simulation per constraint. For the production run, isothermal-isobaric ensemble was considered. The van der Waals cut-off distance was 1.4 nm and the particle mesh Ewald was applied for the long range electrostatic interactions. At each temperature, the averaged force over the set of constraints was determined. One dimensional PMF was then obtained for C6S-PPBS complex by integrating the mean force on the distance constraint range. The corresponding logarithm of the association constant was calculated by integrating the PMF ($\omega(r)$) as defined by Bjerrum et al. [44-45],

$$K_a = 4\pi \int_0^c r^2 e^{-\omega(r)/RT} \, dr \qquad (4)$$

where r is in $(1660^{(1/3)})$ Å unit [45], T in Kelvin and R the Boltzmann constant is set to $8.31*10^{-3}$ kJ/K/mol.

Results and discussion

To investigate the effect of temperature on the interaction between C6S and LDL, and between C6S and PPBS, the association constant K_a was calculated at different temperatures. The effect of temperature on a lipid-protein assembly and on the protein fragment was then probed by exploiting three methods, QCM, PF-ACE and MD. The studies were focused especially on temperatures above 37.0 ºC, and the results obtained with different approaches were compared with each other.

Quartz crystal microbalance. The sensorgrams characterizing LDL-C6S interaction at 37.0 ºC, 38.0 ºC, 39.0 ºC and 40.0 ºC are presented in Fig. 2. The determination of log K_a was achieved by the calculation of estimated values of adsorption k_a and desorption k_d rate constants, (see procedure in *supplementary information*). Preliminary kinetic analysis on the

13

temperature effect on the affinities log K_a values were performed. The calculated log K_a ranged from 10.1 to 11, with a root mean square deviation (RSD) varying from 37 to 54 %. However, we should keep in mind that hydrophobic chains of 11-MUA linker used to attach C6S to gold chip might have strengthened the LDL-PG interaction resulting in slightly higher log K_a value compared that found in the literature [1]. In addition, the model fits on the QCM data yielded large deviations due to noisy desorption curves. One hypothetic reason for such noise could be the increased viscosity with temperature increase.

Qualitative analysis of log K_a=f(T) plot shows a temperature-dependent affinity of C6S-LDL interaction, with a non-linear behavior of the affinities as a function of temperature. A significant decrease of affinity was observed from 37.0 to 38.0 °C followed by an increase of affinity from 38.0 to 39.0 °C and again a decrease.

To verify the previously mentioned non-linear trend of the affinity with temperature, the second experimental technique PF-ACE was employed.

Partial filling capillary electrophoresis. Similarly to QCM experiments, the temperature effect was investigated at the temperatures 37.0, 38.0, 39.0 and 40.0 °C. The capillary column coated with P2QVP-b-PEO was partially filled with C6S for 1, 2, 3, 4, 5 and 6 seconds. LDL and C6S were moving to the same direction, but since the mobility of LDL was much lower, C6S reached LDL for the complex formation. Fig. 3 demonstrates the electropherogram of the complex, and that of the non-bound LDL and C6S. The migration time of LDL − C6S complex decreased linearly as a function of the enhanced amount of negatively charged C6S, and the increased peak height of C6S related to the enhanced filling time corresponded to the excess C6S. The relative migration times of the complex and LDL were included in the calculation of the affinity constants, see Eq. 3. A non-linear behavior of log K_a as function of temperature was in agreement with the QCM results showing the similar qualitative variation of log K_a as a function of temperature.

QCM and AED-derived data. The numerous reports on the role of PPBS in the binding of proteoglycans to LDL [19] confirm PPBS to be a good candidate for our temperature study. Detailed studies using adsorption isotherm determinations were carried out. QCM measurements were performed at seven temperatures 25.0, 28.0, 34.0, 37.0, 38.0, 39.0 and 40.0 ºC. To reduce the experimental noise, each adsorption isotherm data point was determined three times. All the adsorption isotherm fits and AED-calculations are presented together in an overlaid style in Fig.4. The regression coefficients for the best fits at each temperature were: 0.86 (25.0 °C), 0.89 (28.0 °C), 0.90 (34.0 °C), 0.92 (37.0 ° C), 0.94 (38.0 °C), 0.94 (39.0 °C) and 0.95 (40.0 °C).

In the range of 25.0-40.0 ºC, the adsorption isotherms were convex upwards, type I (Figs. 4a and 4b). Moreover, the AEDs calculated (Fig. 4c) exhibited only one distribution at the temperatures between 25.0 and 39.0 ºC, which facilitated the choice of model fit of the adsorption data. All Scatchard plots (not shown), were linear except for 40.0 ºC where the plot was slightly non-linear. Both the Tóth and Langmuir adsorption models were fitted to the experimental data. The Tóth model delivered a heterogeneous index equal to 1, meaning that Tóth model is identical to the Langmuir model. Therefore the Langmuir model was used for these cases. At 40.0 ºC the AED was bimodal, see insert in Fig. 4c, with an unresolved low energy site, the simplest bimodal model bi-Langmuir were found to describe the data well.

As can be seen in Fig 4c, the equilibrium constant is strongly dependent on the temperature. Initially the adsorption energy decreases with increasing temperature to a minimum at 38.0 ºC, thereafter the adsorption energy starts to increase again.

To better illustrate this temperature-dependent behavior, the equilibrium constant fits are presented as a van't Hoff plot, see Fig.5. We see that the van't Hoff plot has a linear part at temperatures up to around 38.0 ºC, and after 38.0 ºC it starts to become non-linear. A non-linear van't Hoff plot means that the change in the interaction enthalpy ΔH is a function of

temperature, reflecting possible structural changes of solute or adsorbent. Changes in the enthalpy with temperature also reflect changes in the heat capacity ΔCp. As has been pointed out by Licata et al. [46], Gibbs-Helmholtz plot, displaying ΔG as a function of temperature, is a better approach for analyzing the temperature dependence of reactions on ΔCp. In our case a concave down Gibbs-Helmholtz plot (not included) obtained reflects a positive ΔCp for the binding of PPBS with C6S. The adsorption energy, calculated for the adsorption process in the temperature range from 25.0 to 38.0 ℃; was -52.4 kJ/mol which indicates that the interactions correspond to non-covalent binding, such electrostatic interaction. Using the Arrhenius equation, and assuming constant pre-exponential factor, the average adsorption energy at 39.0 and 40.0 $^{\circ}$C was around 53 kJ/mol. This shows that the adsorption process is exothermic up to around 38.0 ℃ and turns to endothermic at temperatures higher than 38.0 ℃ meaning that the production of heat at higher temperature is favorable and presumably accelerates the interaction. Interestingly, this temperature region also corresponds to a range where the interaction turns heterogenic. In particular at 40.0 ℃ the AED calculations demonstrate a bimodal interaction with two adsorption sites with log K_a, 4.8 and 3.4, respectivly.

Molecular dynamics insight. PMF calculations for the C6S-PPBS complex were derived from MD simulations at seven temperatures around physiological temperature: 28.0, 34.0, 38.0, 38.5, 39.0, 39.5, and 40.0 ℃. Taking advantages of the freedom inherent in MD parameter setting compared to experiment, 38.5 and 39.5 ℃ were also chosen to give a more detailed view of the non-linear behavior observed experimentally. The PMF plots are depicted in Fig.6.

The PMF curve shapes and patterns are often representatives of the potential contribution. In addition, the PMF depth relates to the free energy of binding and reflects the strength of the

interaction. Visualization of the simulation trajectories at the minimum of the PMF, at each temperature, clearly put in evidence the contribution of the salt to the potential. This contribution is reflected on the PMF by the large minimum and in particular the separated shallow minima in the PMF plots (see Fig. 6). At 40.0 °C, the separated minima proved also to be derived from H-bonded water bridging PPBS and C6S. Details of the energy contributions to C6S-PPBS interaction demonstrates that while at 37.0 °C the electrostatic interaction was twice stronger than the Lennard-Jones contribution, at temperatures above 37.0 °C the difference was much smaller enhancing the contribution of van der Waals interaction at higher temperature.

The logarithm of the association constant, log K_a, was determined by integrating the PMF according to Eq. 6. The plot of log K_a as a function of temperature, presented in Fig. 7, shows a strong temperature-dependence behavior. Two groups are highlighted, group 1 at temperatures from 28.0 to 37.0 °C and group 2 at temperatures above 37.0 °C. For group 1, no significant change in log K_a appeared and the averaged log K_a value was 7. A linear behavior matching qualitatively the QCM experiments data trend was observed. As described earlier [18], the higher log K_a values obtained in MD for C6S-PPBS compared to those achieved by QCM could be attributed to the higher relaxation time, e.g. longer interaction time between the two molecules, and to the consideration of a starting helical structure for PPBS, which was previously shown to favor maximum salt bridges formation [18,40]. For temperatures above 37.0 °C, a non-linear behavior of log K_a is obtained and the interaction proved to be significantly affected even with small temperature change. A peculiar point associated to the highest log K_a was found at 39.5 °C. Checking possible reasons of such strong binding, we looked at the persistence of the salt bridges over the simulation time on the temperature range 37.0-40.0 °C. It appears that 39.5 °C is the only temperature for which all three salt bridges, K3363-CO_2^-(III), R3364-SO_4^-(II), and K3367-CO_2^-(III) involving lysine 3363 and 3367 and

arginine 3364 in disaccharides II and III of PPBS, are persistent continuously and simultaneously throughout the simulation time. It was noticed in these salt bridges that lysine groups bind carboxylate groups while arginine clearly favors sulfate groups.

In order to localize possible structural changes in C6S and PPBS generated by the temperature increase above 37.0 ℃, the root mean-square with least square fitting (rmsd) at the minimum of the PMF was monitored as a function of temperature. The relative structural change, which is the rmsd of C6S compared to the one of PPBS, demonstrated the highest structural changes at 38.0, 39.0, and 39.5 ℃. They also correspond to the temperatures having the largest minimum in the PMF. In addition, though structural deviation of PPBS is observed, the overall helical structure of PPBS is conserved at the minimum of PMF while it is clearly vanishing at large distance from C6S and C6S showed slightly higher rmsd than PPBS at all temperatures. However, further MD with large-scale simulation time should be performed for more detailed study on the structural modification with temperature.

The three exposed methods showed non-linear behavior of the affinity constant above 37.0 ℃. This behavior was observed at the LDL level but as well at the PPBS level. In all the cases, it appears that the interaction is affected by temperature and temperatures above 38.0 ℃ lead to stronger affinity of LDL to C6S. Figure 8 summarizes the results achieved for the interaction of C6S with LDL and PPBS by QCM, PF-ACE and MD and gives a clear picture of the non-linear behavior of the interaction with temperatures above the physiological temperature. Our preliminary experiments on the temperature effect of dermatan glycosaminoglycan interacting with an apolipoprotein E fragment analog of PPBS, have shown also non-linear behavior at temperatures above 37.0 ℃. This raises new interrogation as whether the non-linear behavior observed put in evidence a specificity of

glycosaminoglycans. Further glycosaminoglycan interaction studies are needed to clarify the effect of the temperature.

Conclusions

Two experimental methods, QCM and PF-ACE methods were successfully combined with MD-calculations to probe the temperature effect on the interaction of C6S with LDL and with one of the most important segment of apoB-100, PPBS. A peculiar behavior of the interaction strength upon temperature increase was obtained with a clear non-linear pattern at the temperature range 38.0-40.0 ℃. Two main phenomena were observed, a decrease of affinity from 37.0 ℃ to 38.0 ℃, and an increase of affinity beyond 38.0 ℃. The temperature seemingly affected the interaction of C6S with LDL and PPBS either by influencing the behavior of glycosaminoglycan C6S and/or that of LDL. Atomistic insight into PPBS-C6S interaction showed that C6S has a slightly higher structural variation at all temperatures. However, further studies are needed for the elucidation of the detailed changes in C6S and LDL structural behavior above physiological temperature.

Ethics

In this study, low-density lipoproteins were isolated from plasma obtained from the Finnish Red Cross (permission no 25/2011).

Acknowledgments

References

[1]   G. Camejo, S. Olofsson, F. Lopez, P. Carlsson, G. Bondjers, Identification of Apo B-100 segments mediating the interaction of low density lipoproteins with arterial proteoglycans, *Arterioscler. Thromb. Vasc. Biol.* 8 (1988) 368-377.

[2]   K.J. Williams, I. Tabas, Lipoprotein retention and clues for atheroma regression, *Arterioscler. Thromb. Vasc. Biol.* 25 (2005) 1536-1540.

[3]   K. Skålen, M. Gustafsson, E.K. Rydberg, M. Hultén, O. Wiklund, T.L. Innerarity, J. Borén, Subendothelial retention of atherogenic lipoproteins in early atherosclerosis, *Nature.* 417 (2002) 750-754.

[4]   S. Uesaka, Y. Nakayama, K. Yoshihara, H. Ito, significance of chondroitin sulfate in the synovial fluid of osteoarthritis patients, *J.Orthop. Sci.* 7 (2002) 232-237.

[5]   J. Takeuchi, M. Sobue, E.Sato, M. Shamoto, K. Miura, S. Nakagaki. Variations in glycosaminoglycan components of breast tumors, *Cancer res.* 36 (1976) 2133-2139.

[6]   S.S. Skandalis, M. Stylianou, D.H.Vynios, N.Papageorgakopoulou,D.A. Theocharis, The structural and compositional changes of glycosaminoglycans are closely associated with tissue type in human laryngeal cancer, *Biochimie* 89 (2007) 1573-1580.

[7]   G. Camejo, E. Hurt-Camejo, O. Wiklund, G. Bondjers, Association of apo B lipoproteins with arterial proteoglycans: pathological significance and molecular basis, *Atherosclerosis*. 139 (1998) 205-222.

[8]   K. Öörni, M.O. Pentikäinen, M. Ala-Korpela, P.T. Kovanen, Aggregation, fusion, and vesicle formation of modified low density lipoprotein particles: molecular mechanisms and effects on matrix interaction, *J. Lip. Res.* 41 (2000) 1703-1714.

[9] M.O. Pentikäinen, K. Öörni, M. Ala-Korpela, P.T. Kovanen, Modified LDL - trigger of atherosclerosis and inflammation in the arterial intima, *J Intern Med.* 247 (2000) 359-370

[10]   G.K. Hansson, A. Hermansson, The immune system in atherosclerosis, *Nat Immunol.* 12 (2011) 204-212.

[11]   L.M. Hultén, M. Levin, The role of hypoxia in atherosclerosis, *Curr. Opin. Lipidol.* 20 (2009) 409-414.

[12]   J.C. Sluimer, M.J. Daemen, Novel concepts in atherogenesis: angiogenesis and hypoxia in atherosclerosis, *J Pathol.* 218 (2009) 7-29.

[13]   M. Madjid, K. Toutouzas, C. Stefanadis, J.T. Willerson, S.W. Casscells, Coronary thermography for detection of vulnerable plaques, *J. Nucl. Cardiol.* 14 (2007) 244-249.

[14]   M. Madjid, J.T. Willerson, S.W. Casscells, Intracoronary thermography for detection of high-risk vulnerable plaques, *J. Am. Coll. Cardiol.* 47 (2006) C80-85.

[15]   M. Naghavi, R. John, S. Naguib, M.S. Siadaty, R. Grasu, K.C. Kurian, W.B. van Winkle, B. Soller, S. Litovsky, M. Madjid, J.T. Willerson, W. Casscells, pH Heterogeneity of human and rabbit atherosclerotic plaques; a new insight into detection of vulnerable plaque, *Atherosclerosis.* 164 (2002) 27-35.

[16]   M. Madjid, M. Naghavi, B.A. Malik, S. Litovsky, J.T. Willerson, W. Casscells, Thermal detection of vulnerable plaque, *Am. J. Cardiol.* 90 (2002) 36L-39L.

[17] M. Sneck, P.T. Kovanen, K. Öörni, Decrease in ph strongly enhances binding of native, proteolyzed, lipolyzed, and oxidized low density lipoprotein particles to human aortic proteoglycans, *JBC* 280 (2005) 37449–37454.

[18] K. Lipponen, P.W. Stege, G. Cilpa, J. Samuelsson, T. Fornstedt, M.-L. Riekkola, Three different approaches for the clarification of the interactions between lipoproteins and chondroitin-6-sulfate, *Anal. Chem.* 83 (2011) 6040-6046.

[19] J. Bóren, K. Olin, I. Lee, A. Chait, T.N. Wight, T.L. Innerarity, Identification of the principal proteoglycan-binding site in LDL, J. Clin. Invest. 101 (1998) 2658-2664.

[20] L. D'Ulivo, J. Witos, K. Öörni, P.T. Kovanen, M.-L. Riekkola, Capillary electrochromatography: a tool for mimicking collagen surface interactions with apolipoprotein B-100 peptides, *Electrophoresis.* 30 (2009) 3838-3845.

[21] L. D'Ulivo, J. Saint-Guirons, B. Ingemarsson, M.-L. Riekkola, Quartz crystal microbalance, a valuable tool for elucidation of interactions between apoB-100 peptides and extracellular matrix components, *Anal. Bioanal. Chem.* 396 (2010) 1373-1380.

[22] Y. Song, Z. Li, Z. Liu, G. Wei, L. Wang, L. Sun, Immobilization of DNA on 11-Mercaptoundecanoic acid-modified gold (111) surface for atomic force microscopy imaging. *Microsc. Res. Tech.* 68 (2005) 59-64.

[23] R. J. Havel, H. A. Eder, J. H. Bragdon, The distribution and chemical composition of ultracentrifugally separated lipoproteins in human serum, *J. Clin. Invest.* 34 (1955) 1345-1353.

[24] C. M. Radding, D. Steinberg, Studies on the synthesis and secretion of serum lipoproteins by rat liver slices, *J. Clin. Invest.* 39 (1960) 1560-1569.

[25] O. H. Lowry, N. J. Rosebrough, A. L. Farr, R. J. Randall, Protein measurement with the Folin phenol reagent, *J. Biol. Chem.* 193 (1951) 265-275.

[26]   G. Sauerbrey, The use of quartz crystal oscillators for weighing thin layers and for micro-weighing, *Z. Phys.* 155 (1959) 206-222.

[27]   D. G. Myszka, T.A. Morton, Clamp: a biosensor kinetic data analysis program, *Trends in Biochem. Sci.* 23 (1998)149-150.

[28]   G. Guiochon, A. Felinger, D. G. Shirazi, A. Katti, Fundamentals of Preparative and Nonlinear Chromatography, 2nd edition. Elsevier Academic Press, San Diego, CA, 2006.

[29]   G. Götmar, J. Samuelsson, A. Karlsson, T. Fornstedt, Thermodynamic characterization of the adsorption of selected chiral compounds on immobilized amyloglucosidase in liquid chromatography, *J. Chromatogr. A*. 1156 (2007) 3-13.

[30]   R. Arnell, N. Ferraz, T. Fornstedt, Analytical Characterization of Chiral Drug-Protein Interactions: Comparison between the Optical Biosensor (Surface Plasmon Resonance) Assay and the HPLC Perturbation Method, *Anal. Chem.* 78 (2006) 1682-1689.

[31]   P. Sandblad, R. Arnell, J. Samuelsson, T. Fornstedt, Approach for reliable evaluation of drug proteins interactions using surface plasmon resonance technology, *Anal. Chem.* 81 (2009) 3551-3559.

[32]   B. J. Stanley, S. E. Bialkowski, D. B. Marshall, Analysis of first-order rate constant spectra with regularized least-squares and expectation maximization. 1. Theory and numerical characterization, *Anal. Chem.* 85 (1993) 259-267.

[33]   X. Zhang, J. Samuelsson, J.-C. Janson, C. Wanga, Z. Suc, M. Guc, T. Fornstedt, Investigation of the adsorption behaviour of glycine peptides on 12% cross-linked agarose gel media, *J. Chromatogr. A*. 1217 (2010) 1916-1925.

[34]   K. Lipponen, S. Tähkä, M. Kostiainen and M.-L. Riekkola, manuscript (2013).

[35]   B. A. Williams, G. Vigh, Fast, accurate mobility determination method for capillary electrophoresis, *Anal. Chem.* 68 (1996) 1174-1180.

[36]   A.-J. Wang, K. Vainikka, J. Witos, L. D'Ulivo, G. Cilpa, K. Öörni, P. T. Kovanen, M.-L. Riekkola, Partial filling affinity capillary electrophoresis with cationic poly(vinylpyrrolidone)-based copolymer coatings for studies on human lipoprotein-steroidinteractions, *Anal. Biochem.*, 399 (2010) 93-101.

[37]   G. Yohannes, M. Jussila, K. Hartonen, M.-L. Riekkola, Asymmetrical flow field-flow fractionation technique for separation and characterization of biopolymers and bioparticles, *J. Chromatogr. A* 1218 (2011) 4104–4116.

[38]   G. Cilpa, M.T. Hyvönen, A. Koivuniemi, M.-L. Riekkola, Atomistic insight into chondroitin-6-Sulfate glycosaminoglycan chain through quantum mechanics calculations and molecular dynamics simulation, *J. Comp. Chem.* 31 (2010) 1670-1680.

[39]   Accelrys Discovery Studio 2.1; Accelrys: San Diego, CA. http://www.accelrys.com.

[40]   G. Cilpa, A. Koivuniemi, M.T. Hyvönen, M.-L. Riekkola, A Molecular Dynamics Approach for the Association of ApolipoproteinB-100 and Chondroitin-6-sulfate, *J. Phys. Chem. B.* 115 (2011) 4818-4825.

[41]   B. Hess, C. Kutzner, D. Van der Spoel, E. Lindahl, GROMACS 4: Algorithms for highly efficient, load-balanced, and scalable molecular simulation*, J. chem. Theory Comput.* 4 (2008) 435-447.

[42]   H.J.C. Berendsen, J.P.M. Postma, W.F. van Gunsteren, J. Hermans, Interaction models for water in relation to protein hydration, In Intermolecular forces; Ed. B. Pullman, Reidel, Dordrecht, The Netherlands, (1981) 331-342.

[43]   G.T. Ibragimova, R.C. Wade, Importance of explicit salt ions for protein stability in molecular dynamics simulation, *Biophys. J.*, 74 (1998) 2906–2911.

[44]   M.-C. Justice, J.-C. Justice, Ionic interactions in solutions. I. the association concepts and the McMillan-Mayer theory, *J. Sol. Chem.* 5 (1976) 543-561.

[45]   Y. Zhang, J.A. McCammon, Studying the affinity and kinetics of molecular association with molecular-dynamics simulation, *J. Chem. Phys.* 118 (2003) 1821-1827.

[46]   V.J. Licata, C.-C. Liu, Analysis of free energy versus temperature curves in protein folding and macromolecular interactions, *Methods Enzymol.*, 488 (2011) 219-238.

Figure captions

Figure 1. Illustration of (a) the Scatchard plot and (b) the corresponding adsorption energy distribution calculations for three different adsorption datasets. Dataset 1 is a Langmuir adsorption model, Dataset 2 a Tóth model and Dataset 3 a bi-Langmuir model.

Figure 2. Sensorgrams for C6S-LDL interaction att different temperaturs giving the response (*R*) as a function of time in second(s).

Figure 3. Illustration of the electropherogram obtained at 37,0 ºC displaying the migration time variation of C6S-LDL complex as a function of filling time of C6S (1, 2, 3, 4, 5 and 6 s) in P2QVP-*b*-PEO coated capillary. In inset is presented the linear fitting of the migration time of the complex as a function of filling time of C6S. The slope of that fit is needed to calculate K_a (see Eq. 3). Running conditions: L_{tot} 38.5cm, L_{det} 30cm, separation voltage 25 kV, LDL injection for 2 s at 50 mbar, UV-detection at 200nm, LDL solution (0.1 mg/mL), C6S solution (0.6 mg/ml), BGE- phosphate buffer (pH 7.4, ionic strength 20 mM).

Figure 4. Adsorption isotherms for C6S-PPBS interaction at temperatures 25.0 C,28.0 C, 34.0 C, 38.0, 39.0, and 40.0 C is plotted for (a) a low and (b) a high analyte concentration range. In (c) the corresponding AED-calculations are plotted; the inset shows the bimodal distribution at 40.0ºC.

Figure 5. Demonstration of van't Hoff plots for the equilibrium constants from the C6S-PPBS adsorption obtained from the adsorption isotherm fits (circles) and AED-calculation

25

(squares). The solid line displays the linear fit for the equilibrium data from model fit for up to 38.0ºC and the dashed line displays only the high temperature range, i.e. data acquired at 38.0 – 40.0ºC.

Figure 6. PMF plots as a function of intermolecular distances at six temperatures in the range 37.0-40.0ºC. The reported PMF at 37.0ºC was calculated previously [18]. In inset is included a zoom of the long range shallow minima of the PMF at 40.0ºC.

Figure 7. PMF-derived log K_a values at temperatures 28.0, 34.0, 37.0, 38.0, 38.5, 39.0, 39.5, 40.0ºC. Two groups are highlighted with (1) linear and (2) non-linear behavior.

Figure 8. Log K_a as a function of temperature at 37.0, 38.0, 39.0, 40.0ºC a) for LDL-C6S interaction by QCM, b) for LDL-C6S interaction by PF-ACE   c) for PPBS-C6S interaction by QCM, d) for PPBS-C6S interaction by MD at 37.0, 38.0, 38.5, 39.0, 39.5, 40.0ºC. The dotted line corresponds to the plot without 38.5 and 39.5 ºC similar to the cases a), b) and c).
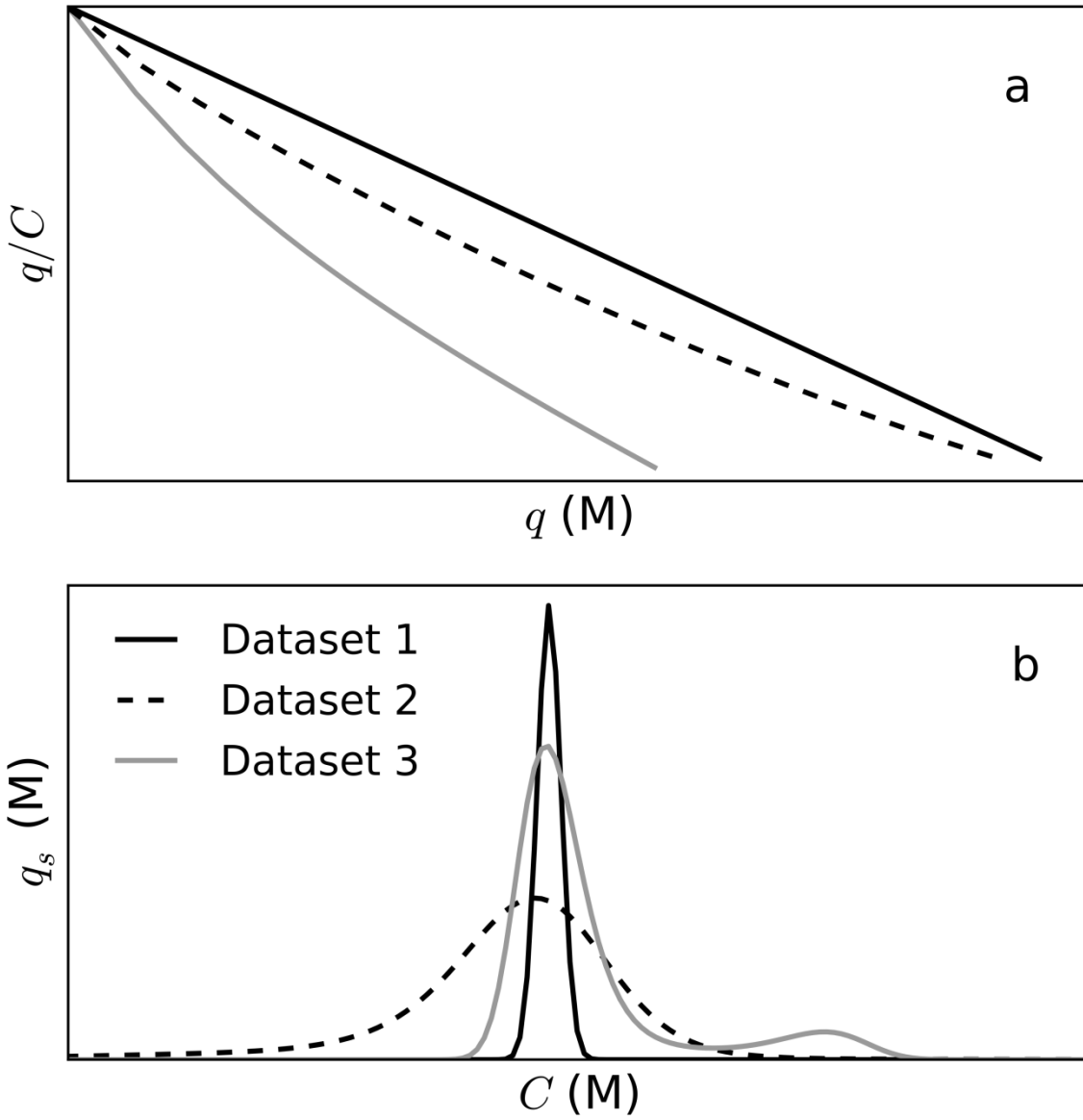
Fig. 1
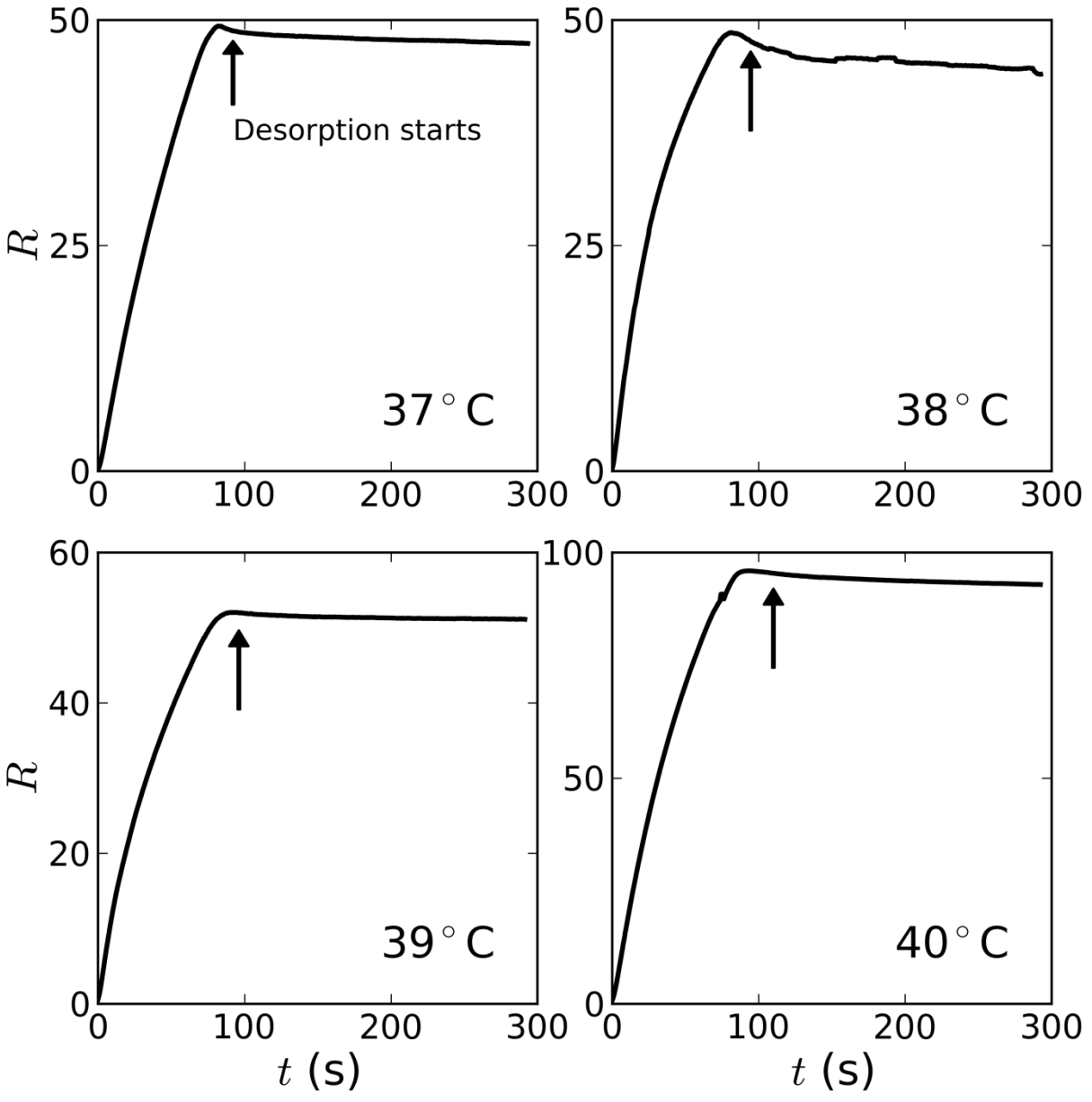
Fig. 2
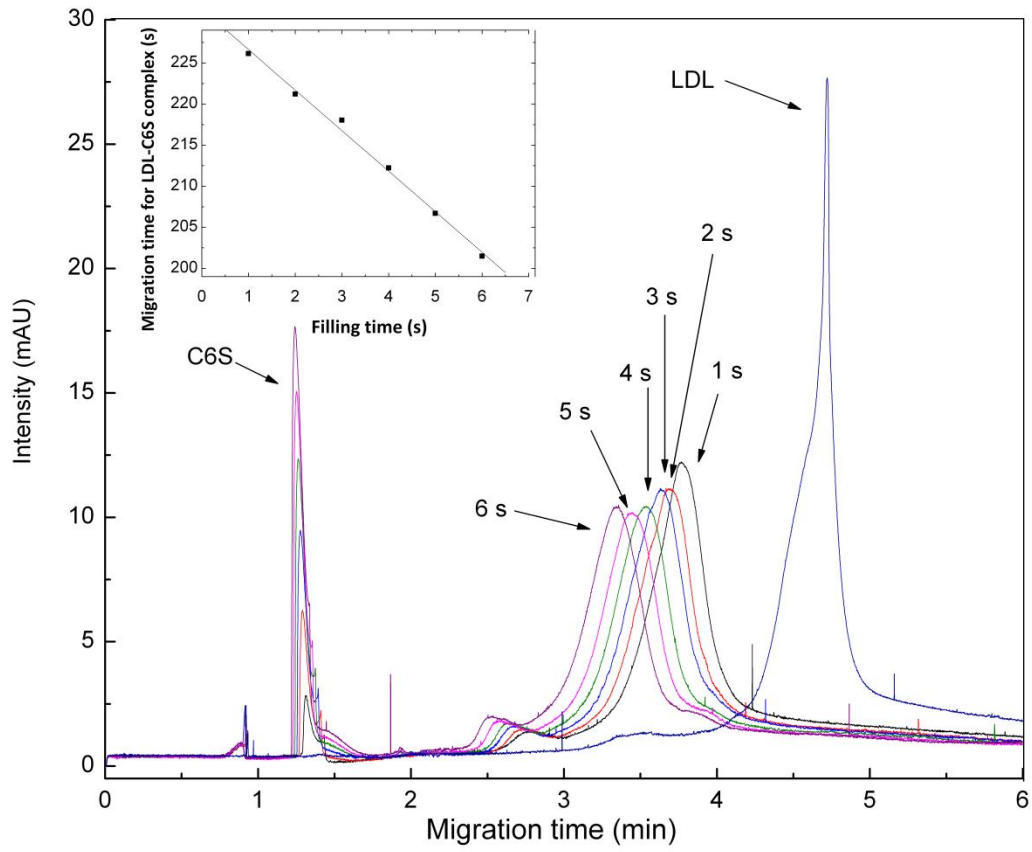
Fig. 3
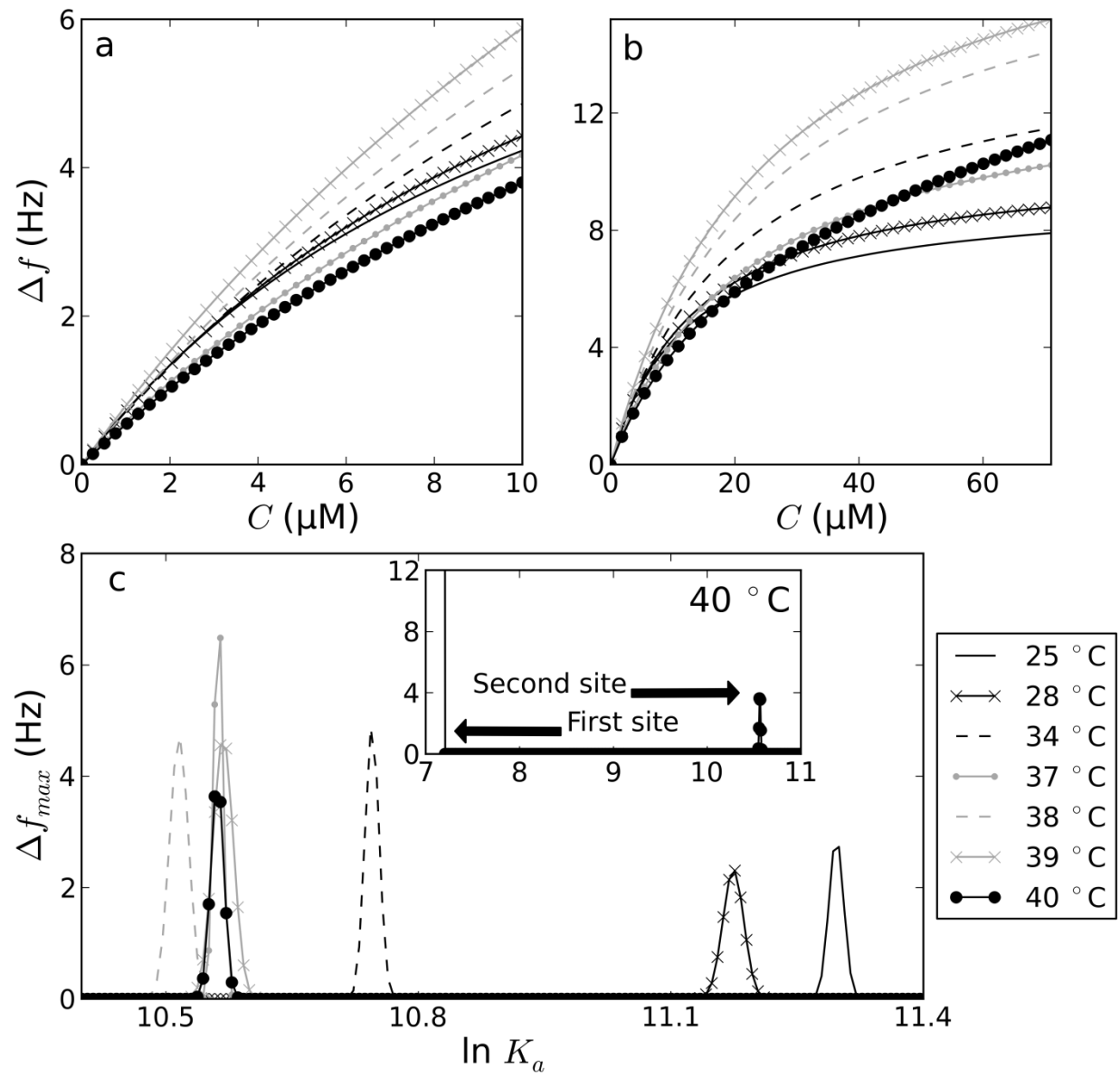
Fig. 4
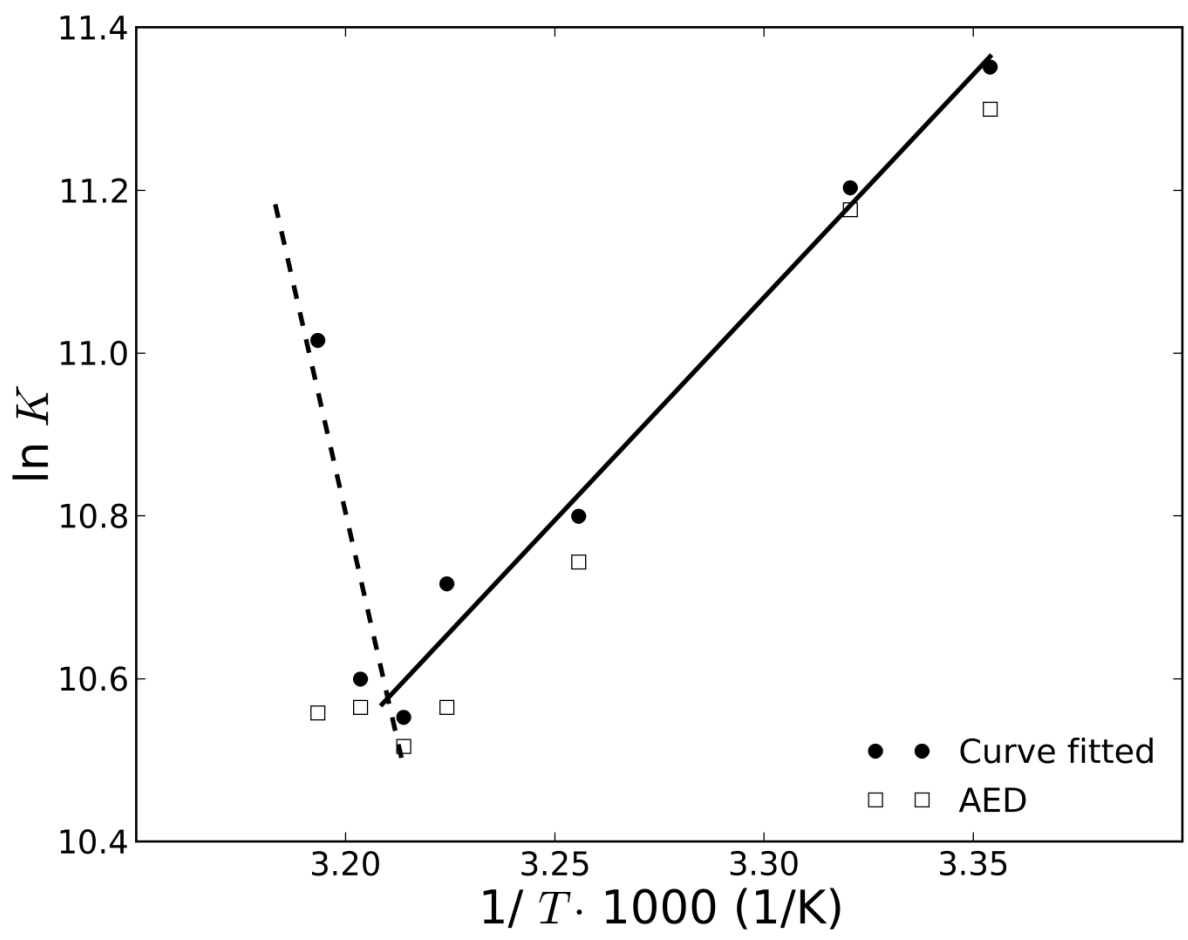
Fig. 5
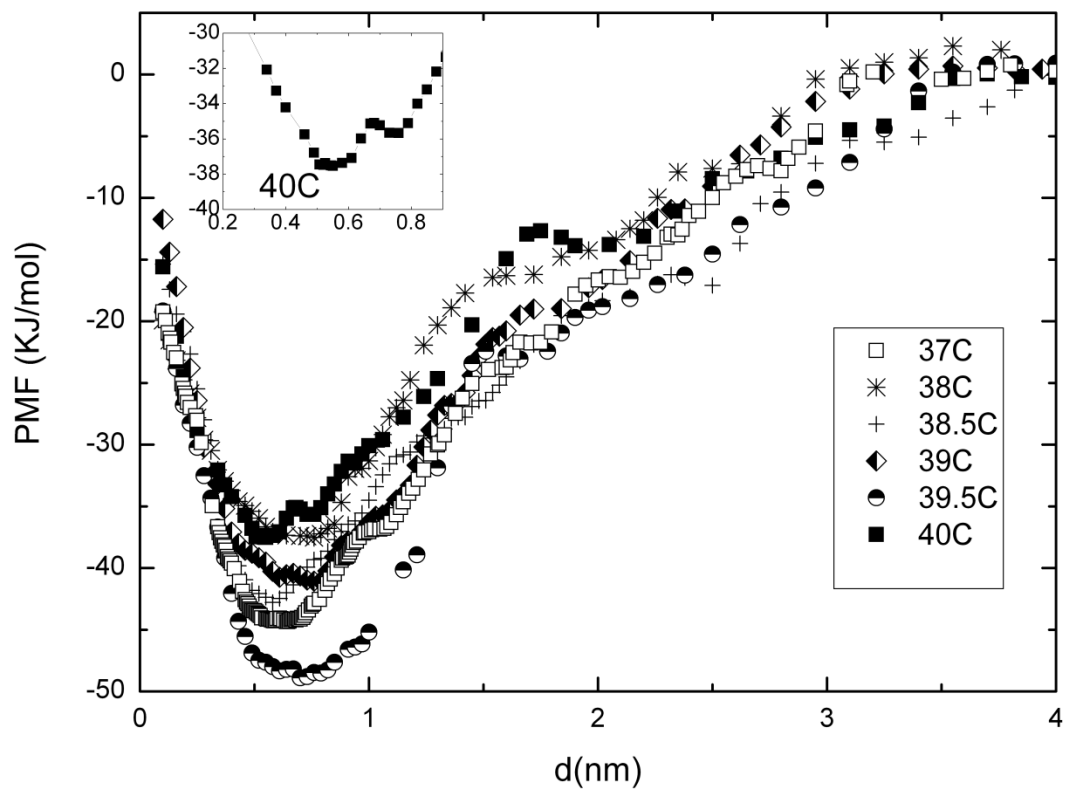
Fig. 6
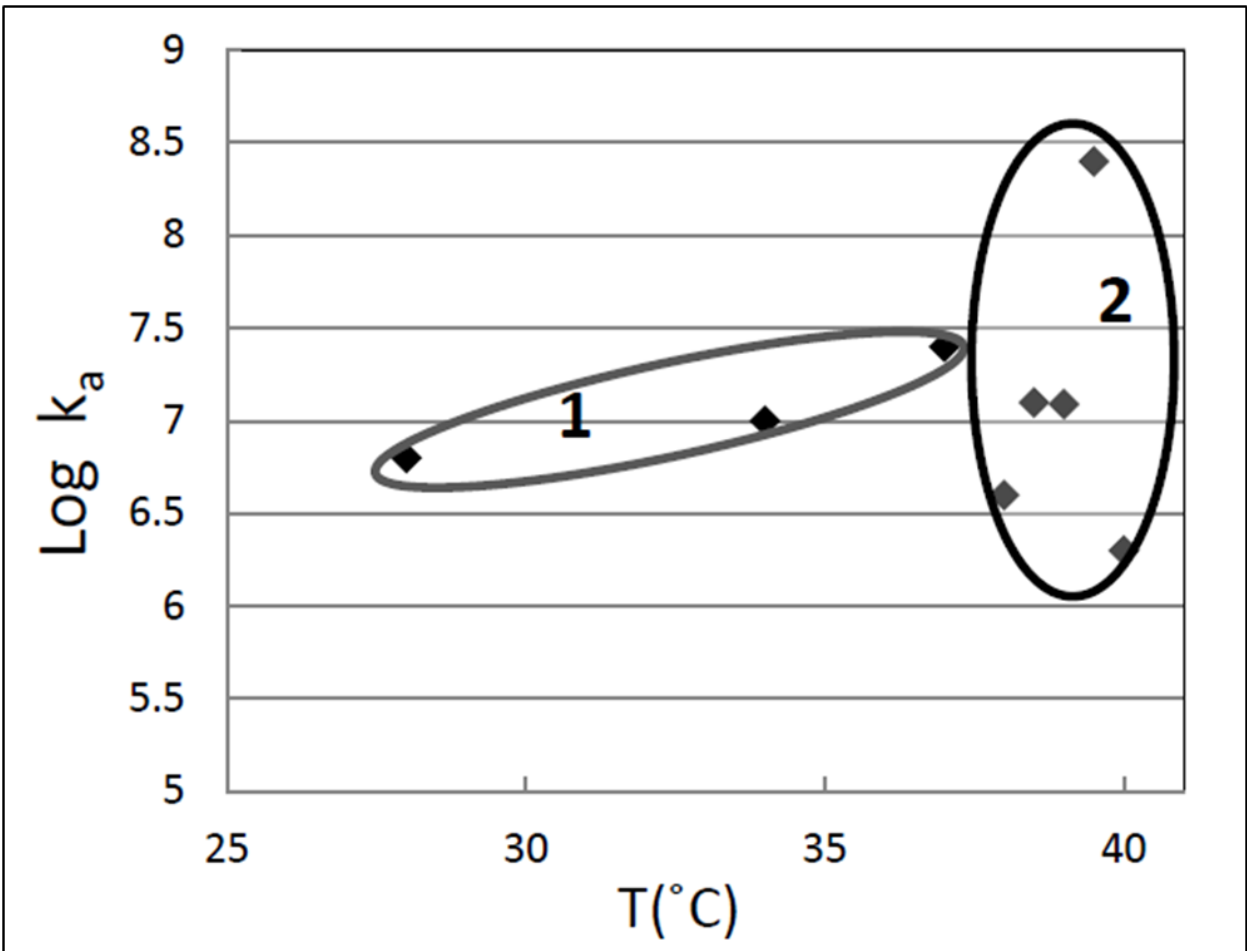
Fig. 7
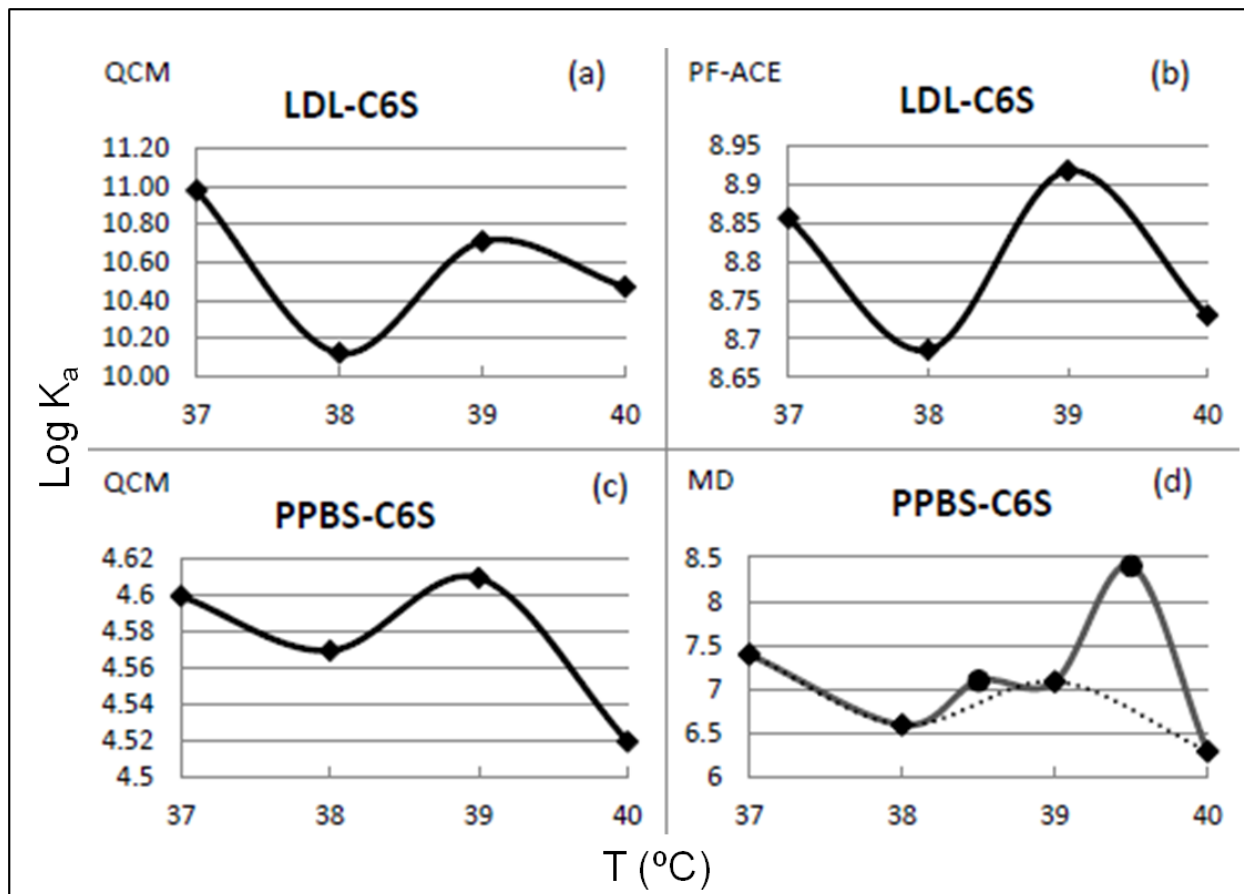
Fig. 8

Three complementary techniques for the clarification of temperature effect on low-density lipoprotein-chondroitin-6-sulfate interaction

Geraldine Cilpa-Karhu[a]*, Katriina Lipponen[a], Jörgen Samuelsson[b], Katariina Öörni[c], Torgny Fornstedt[b], Marja-Liisa Riekkola[a]*

[a]Laboratory of Analytical Chemistry, Department of Chemistry, P.O. Box 55, FIN-00014 University of Helsinki, Helsinki, Finland, [b]Department of Engineering and Chemical Sciences, Karlstad University, SE-651 88 Karlstad, Sweden and [c]Wihuri Research Institute, Haartmaninkatu 8, FIN-00290 Helsinki, Finland

Supplementary information

In this section we will present:

- The in-house made program for calculation of equilibrium constants from classical kinetic relationships.

- Raw adsorption data from the PPBS-C6S adsorption measurements used for the adsorption isotherms.

- The calculated entropy, enthalpy and Gibbs free energy using the Gibbs-Helmholtz equation.

The in-house program,

The in-house written program that describes a simple ligand analyte adsorption desorption process is based on this simple assumptions:

The reaction we studied are defined as

$$[A] + [L] \underset{k_d}{\overset{k_a}{\Leftrightarrow}} [AL], \tag{1}$$

where k_d and k_a are the desorption and adsorption rate constants. [A], [L] and [AL] are concentrations of solute, ligand and adsorbed solute, respectively. The change in [AL] could be expressed as:

$$\frac{d[AL]}{dt} = ka[A] \cdot [L] - kd[AL] \tag{2}$$

Because we measure a response (R), we rewrite eq. 1 using the following relationships:

$$R = \alpha[AL] \tag{3}$$

$$[L] = [L]_0 - [AL] \tag{4}$$

$$R_{max} = \alpha[L]_0 \tag{5}$$

Introducing eq. 3, 4 and 5 into 2 we get:

$$\frac{dR}{dt} = k_a[A]R_{max} - (ka[A] + k_d)R \tag{6}$$

By integration of the rate eq. 6, we obtain:

$$R = [A]k_a R_{max} \frac{1 - e^{-([A]k_a + k_d)t}}{([A]k_a + k_d)} \tag{7}$$

To make calculations simpler we introduce two constants k_1 and k_2 defined as follow:

$$k_1 = ([A]k_a + k_d) \tag{8}$$

$$k_2 = \frac{[A]k_a R_{max}}{k_1} \tag{9}$$

Equation 7 can then be simplified, using eq. 8 and 9:

$$R = k_2 - k_2 e^{-k_1 t} \tag{10}$$

We assume that [A] is kept constant during the adsorption phase. To determine the rate constants we need to carry out several experiments using different solute concentration. One other way is to watch the desorption phase. The dissociation rate is simpler to investigate, we assume that [A] equal zero during this phase. In this case we get the following rate equation:

$$\frac{dR}{dt} = -k_d R \qquad (11)$$

After solving eq. 11 we get:

$$R = R_0 e^{-k_d t} \qquad (12)$$

So by combining results from eq. 10 and 12 we could estimate both rate constants. Dissociation constant (K_D) or association constant ($K_a = 1/K_D$), can be calculated according to $K_D = k_d/k_a$.

Raw adsorption data for C6S- PPBS interaction

All adsorption measurements for the C6S- PPBS interaction were conducted as triplicates. The raw adsorption data are presented in Fig. 1S, below. The symbols are the experimental data and the lines are the model fit. Langmuir model are used for all temperature except at 40 ^{o}C where the Bi-Langmuir models are used.
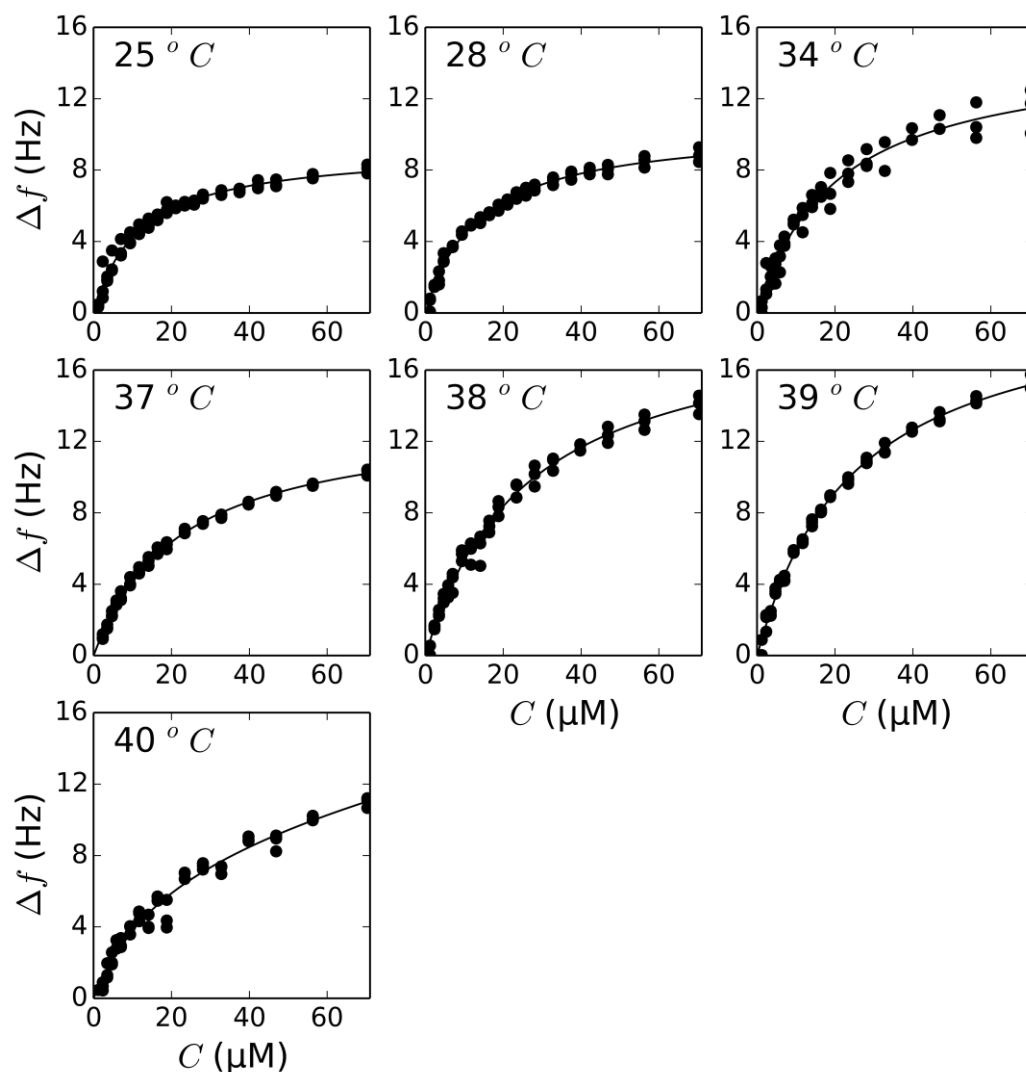
Figure 1S: Raw adsorption isotherm data for C6S-PPBS interaction at temperatures 25.0, 28.0, 34.0, 38.0, 39.0 and 40.0 ^{o}C. Experimental points (full dots), including the 3 repeats at each concentration and model fit (line) are displayed.

Gibbs-Helmholz

In Figure 5, we see that the enthalpy is dependent on the temperature (straight line indicates constant enthalpy); we need to use a models what could handle this. The Gibbs-Helmholz equation does not assume constant enthalpy in the adsorption process. The form of Gibbs-Helmholz we use only assumes that the heat capacity is constant (ΔC_p). One could state these equations as [1]:

$$\Delta G(T) = \Delta H_r - T\Delta S + \Delta C_p\left(T - T_r - T \cdot \ln\left(\frac{T}{T_r}\right)\right) \tag{13}$$

$$\Delta H(T) = \Delta H_r + \Delta C_p\left(T - T_r\right) \tag{14}$$

$$\Delta S(T) = \Delta S_r + \Delta C_p \cdot \ln\left(\frac{T}{T_r}\right) \tag{15}$$

where the subscript r denote a single selected reference temperature (arbitrary selected).

All calculation was done using Python 2.7.3, numpy 1.6.1, scipy 0.9.0 and matplotlib 1.1.1. All nonlinear fitting were done using the Levenberg-Marquardt algorithm implemented in scipy.

Model fit

The estimated equilibrium constants (high energy site are used at 40 ^{o}C) for the adsorption of PPBS toC6S at different temperature were fitted to eqs. (13-15) and the resulted is fit is plotted in Fig. 2S.
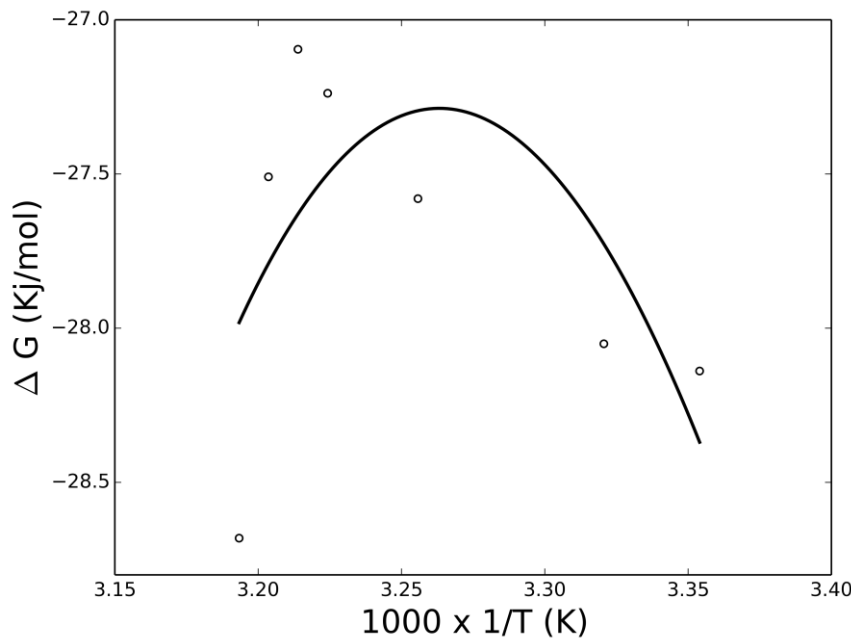
Figure 2S: Gibbs-Helmholtz model fit to C6S-PPBS. Symbols are calculated from equilibrium constants from the model fit, see Figure 1S.

Using the model we could estimate the heat capacity to 9.55 kJ/(mol K) and Gibbs free energy, entropy and enthalpy is presented in Table 1S below.

Table 1S: Estimated Gibbs free energy, enthalpy and entropy for the adsorption of C6S-PPBS at different temperatures

	25 °C	**28 °C**	**34 °C**	**37 °C**	**38 °C**	**39 °C**	**40 °C**
ΔH (kJ/mol)	-28.4	-27.7	-27.3	-27.5	-27.6	-27.8	-28.0
ΔH (kJ/mol)	-106.5	-77.9	-20.6	8.1	17.6	27.2	36.7
ΔS (J/(mol K))	-262.2	-166.5	21.9	114.7	145.4	176.1	206.6

Observe that the model fit presented in Fig. 2S is not good, so no major conclusions could be drawn from this data.

References

[1] V.J. LiCata, C.-C. Liu, in:, J.M.H. and G.K.A. Michael L. Johnson (Ed.), Methods in Enzymology, Academic Press, 2011, pp. 219–238.